phys. stat. sol. (b) **221**, 583 (2000)

Subject classification: 61.72.Bb; 62.20.Fe; S1; S4

Non-Local Plasticity at Microscale: A Dislocation-Based and a Cosserat Model

R. SEDLÁČEK (a) and S. FOREST (b)

(a) Institut für Werkstoffwissenschaften, Lehrstuhl I, Universität Erlangen-Nürnberg, Martensstrasse 5, D-91058 Erlangen, Germany

(b) Centre des Matériaux, CNRS, Ecole des Mines de Paris, UMR 7633, PB 87, F-91003 Evry, France

(Received February 7, 2000; in revised form May 17, 2000)

An interpretation of intrinsic length scale in materials containing plastically soft and hard phases is proposed, based on the idea that dislocations gliding in the soft phase have to bow between the hard phase. Accordingly, the self-energy (line-tension) of the bowing dislocations is introduced into the continuum mechanics description of the plastic deformation. A direct relation between a simple dislocation-based and a Cosserat model is established, allowing for identification of the Cosserat intrinsic length, rotation and curvature. Attention is also paid to the question whether the geometrically necessary dislocations contribute primarily to isotropic or to kinematic hardening.

1. Introduction

At the scale of micrometers, size effects have been observed in various modes of plastic deformation. Roughly speaking, the smaller is some characteristic length associated with the deformation field, the stronger is the response [1]. As classical continuum theories of plasticity cannot describe such effects, non-local theories have been revived recently to account for them. In these strain gradient [1–3] or Cosserat theories [4, 5], intrinsic length scales are introduced for dimensional consistency. The size effect is revealed when the intrinsic length scale is not too different from the characteristic length of the deformation field. The intrinsic length can thus be fitted by comparing predictions of the theory with experimental results [1, 3]. A precise physical interpretation of the intrinsic length scale introduced in this way remains unclear, but the size effects are usually related to the enhanced hardening caused by storage of geometrically necessary dislocations [6], which is directly related to the plastic strain gradients. It is commonly assumed that this additional hardening is similar in nature to the isotropic (forest) hardening caused by statistically stored dislocations, that is, it can simply be related to (the square root of) their scalar density.

In an alternative strain gradient model [7], the size effect in metal-matrix composites has been attributed to the bowing of dislocations between particles. Although no direct relation between the proposed dislocation model [8] and the continuum theory was established, this interpretation is supported by the well known empirical Orowan and Hall-Petch relations between flow stress and obstacle spacing which were found to be valid in various microstructures. Recently, the dislocation density tensor was introduced into the theory [9]. As a result, expressions for the plastic spin and back stress could be

obtained, the latter suggesting that the geometrically necessary dislocations contribute to kinematic hardening.

The purpose of this paper is to elaborate the physical interpretation of the intrinsic length scale in materials containing plastically soft and hard phases and to establish a direct relation between a dislocation-based and a Cosserat model. Also, attention will be paid to the question whether the geometrically necessary dislocations contribute primarily to isotropic or to kinematic hardening. The underlying idea is that in the course of plastic deformation, the dislocations gliding in the soft phase have to bow between the hard phase. Accordingly, the self-energy (line-tension) of the bowing dislocations is introduced into the continuum mechanics description of the plastic deformation. Thus, the intrinsic length scale is related to line tension and density of the bowing dislocations while the characteristic length of the deformation field is given by the spacing between the hard phase. The size effect depends on the ratio between these two lengths.

This concept applies not only to metal-matrix composites or other truly two-phase materials, but even to single crystals of metals which exhibit deformation-induced dislocation structures: cells [10], subgrains [11, 12], persistent slip bands (PSBs) [13–15], veins [16]. Despite of the quite different geometrical arrangements of the above mentioned microstructures, we try to capture the main features common to all of them by means of a case study, utilizing simple one-dimensional models.

The plan of the paper is as follows. In Section 2, a simple dislocation-based model of plastic deformation of a two-phase structure is recalled [17, 18] and completed to account for lattice rotation and curvature. As the model is formulated within the classical framework [14] it accounts for the build-up of back stress in the soft phase, i.e. for kinematic hardening. Being enriched by the assumption that the plastic deformation is carried by curved dislocations, cf. [15, 16], the model accounts also for non-local effects and yields an intrinsic length scale. The numerically computed results of the full model are carefully compared with limit cases which can be solved analytically: (i) a linearized model for mild dislocation bowing (anelasticity) [17, 18], (ii) an Orowan-type model for the full plastic flow, cf. [13, 19], and (iii) the classical composite model [14]. The Cosserat formalism is employed in Section 3 to set up an alternative simple model of non-local plasticity of two-phase materials. By comparison with the linearized dislocation-based model, the intrinsic length scale, rotation and curvature of the Cosserat continuum are interpreted. Basic equations of the continuum theory of dislocations [20] and of Cosserat continuum for small strains and small rotations are summarized in Appendices A and B.

2. Dislocation-Based Model

A two-phase structure consisting of a plastically hard phase and a plastically soft phase is modelled as a one-dimensional periodic elastic–plastic continuum. Single slip is considered for simplicity, Voigt approximation of homogenization theory is utilized, parallel shearing (iso-strain) is assumed. To allow for a non-trivial distribution of stresses even in this one-dimensional formulation, the stress equilibrium is fulfilled only on average. This one-dimensional model thus mimics the behaviour of a non-homogeneous two-dimensional structure with internal stresses, cf. [14].

In the Voigt approximation, only one non-zero component $u_x = \bar{\gamma} y$ of the material displacement field $\mathbf{u}$ is considered, which yields a homogeneous material shear $\bar{\gamma}$ as the

only non-zero component of the material displacement gradient $\boldsymbol{\beta}$, cf. eq. (A1),

$$\beta_{xy} = \partial_y u_x = \bar{\gamma} \,. \tag{1}$$

The homogeneous – and therefore compatible – material shear $\bar{\gamma}$ is decomposed into its elastic and plastic parts, cf. eq. (A2),

$$\bar{\gamma} = \gamma^{\mathrm{e}}(x) + \gamma^{\mathrm{p}}(x) \,, \tag{2}$$

each of them being in general incompatible. Dislocations must be stored in the non-homogeneously plastically deformed crystal to enable the compatibility of the material shear deformation [20, 21]. The density $\alpha = \alpha_{xz}$ of these geometrically necessary dislocations follows according to eq. (A3) from the elastic shear,

$$\alpha = -\partial_x \gamma^{\mathrm{e}} \,. \tag{3}$$

These continuously distributed dislocations are aligned with the z axis, their Burgers vector is in the x direction. Non-zero components of the elastic strain $\boldsymbol{\varepsilon}^{\mathrm{e}}$ and the elastic rotation $\boldsymbol{\omega}^{\mathrm{e}}$ are, cf. eq. (A4),

$$\varepsilon^{\mathrm{e}}_{xy} = \varepsilon^{\mathrm{e}}_{yx} = \omega^{\mathrm{e}}_{xy} = -\omega^{\mathrm{e}}_{yx} = \frac{1}{2}\,\gamma^{\mathrm{e}} \,. \tag{4}$$

Just one non-zero component $\phi = \phi_z$ of the axial vector of lattice rotation follows according to eq. (A5) from the skew-symmetric tensor of the elastic rotation $\boldsymbol{\omega}^{\mathrm{e}}$,

$$\phi = -\frac{1}{2}\,\gamma^{\mathrm{e}} \,. \tag{5}$$

Lattice curvature $\kappa = \kappa_{zx}$ results from the lattice rotation ϕ, eq. (A6),

$$\kappa = \partial_x \phi \,. \tag{6}$$

Note that plastic rotation and curvature can be defined in an analogous way using the plastic shear strain γ^{p}. However, as the plastic deformation by glide of dislocations causes the material to rotate but not the lattice, the plastic rotation and curvature determine the lattice rotation and curvature only indirectly via the compatibility requirement and the resulting elastic deformation [22].

Because of the one-dimensional formulation of the model, the exact stress equilibrium (A8) would lead to a trivial stress distribution. To mimic a two-dimensional periodic structure with internal stresses, the stress equilibrium is considered only on average. In the case of the periodic arrangement of a soft phase (width s) and a hard phase (width h) sheared in parallel by virtue of an applied stress $\bar{\tau}$, it follows from eq. (A9),

$$\frac{1}{s+h} \int\limits_{\langle s+h \rangle} \tau(x)\,\mathrm{d}x = \bar{\tau} \,, \tag{7}$$

where τ is the shear component of the symmetric stress tensor $\boldsymbol{\sigma}$, eq. (A7),

$$\tau = \sigma_{xy} = \sigma_{yx} \,. \tag{8}$$

The classical framework is completed by Hooke's law for the elastic shear strain,

$$\tau = 2G\,\frac{\gamma^{\mathrm{e}}}{2} \,, \tag{9}$$

G is the elastic shear modulus.

Plastic deformation sets in and continues as long as a local yield stress is exceeded. The yield stresses of the unbounded hard and soft phases fulfil the relation $\hat{\tau}_\mathrm{h} \gg \hat{\tau}_\mathrm{s}$. For the following considerations it is sufficient to assume that the yield stress of the unbounded soft phase is negligible, $\hat{\tau}_\mathrm{s} \approx 0$. The size dependence of the flow stress of the soft phase bounded in the composite will be accounted for by explicitly considering the bowing of dislocations between the hard phase.

2.1 Full curvature model

The plastic shear is supposed to be carried by dislocation loops lying in the xOz glide plane and having the Burgers vector with the only non-zero component $\pm b_x$, Fig. 1. For simplicity, only straight screw parts of the dislocation loops extending across the soft phase at zero applied stress are considered. They cause no long-range internal stresses, for their net Burgers vector vanishes on average. Upon applying a stress increment $\bar{\tau}$, the screw dislocations start to bow out, the soft phase being sheared plastically non-homogeneously. The form of the bowed-out dislocations $\varphi(x)$ is determined by equilibrium of the forces acting on them: the Peach-Koehler force due to the local shear stress $\tau_\mathrm{s}(x)$ and the self-force due to their line tension T,

$$\tau_\mathrm{s}(x)\, b + \frac{T}{R(x)} = 0\,, \tag{10}$$

with $R(x) = (1 + (\partial_x \varphi)^2)^{3/2}/\partial_x^2 \varphi$ being the local radius of curvature of the bowed-out dislocation lines. The increment of plastic shear deformation in the soft phase caused by the bowing-out of the mobile dislocations with density ϱ_m is

$$\gamma_\mathrm{s}^\mathrm{p}(x) = \varrho_\mathrm{m} b\, \varphi(x)\,. \tag{11}$$

As $\hat{\tau}_\mathrm{h} \gg \hat{\tau}_\mathrm{s}$, the hard phase is sheared only elastically. The decomposition (2) combined with Hooke's law (9) then requires

$$\tau_\mathrm{s}(x) = \tau_\mathrm{h} - G\gamma_\mathrm{s}^\mathrm{p}(x)\,. \tag{12}$$

2.1.1 Numerical solution

A simplified version of the numerical method introduced in Ref. [23] has been used to solve the system of eqs. (10), (11) and (12) with the stress equilibrium (7). The dislocation line $\varphi(x)$ is parametrized by the angle u, Fig. 1. The two components of the mapping $(\varphi_x(u), \varphi_y(u))$ are approximated by cubic splines [24], so that the curvature $1/R(u) = (\varphi_x'\varphi_y'' - \varphi_y'\varphi_x'')/\|\varphi'\|^3$ can easily be computed. The analytical solution of the

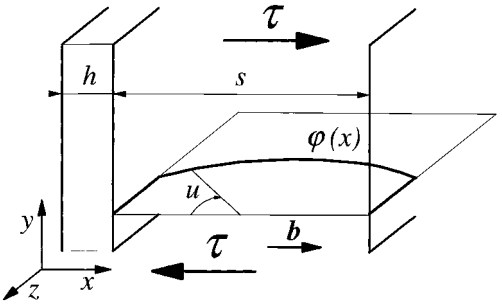

Fig. 1. Sketch of a dislocation bowing between the hard phase. A part of the loop gliding in the xOz plane is shown, with the curved (originally screw) section $\varphi(x)$ and edge segments at the soft/hard phase interface. The resolved shear stress τ, Burgers vector b and the angle u used for parametrization of the dislocation line are indicated

linearized model introduced below is used as an initial estimate of the dislocation shape. Then, the stress $\tau_s(x)$ follows from eqs. (11), (12) and (7), the integration in eq. (7) being performed with the help of the trapezoidal rule [24]. The dislocation shape $\varphi(u)$ and stress $\tau_s(x)$ are updated in small increments until the unbalanced force resulting from the left hand side of eq. (10) is relaxed.

The following model parameters have been used: shear modulus $G = 10\,\text{GPa}$, Burgers vector magnitude $b = 0.1\,\text{nm}$, applied axial stress $\bar{\sigma} = 20\,\text{MPa}$; line tension $T \approx Gb^2$ [25], density of mobile dislocations $\varrho_m \approx (\bar{\sigma}/Gb)^2$ [26], resolved shear stress $\bar{\tau} = \bar{\sigma}/3$. Volume fraction of the hard phase was kept constant at $h/(s+h) = 0.1$, while the width of the soft phase was varied to cover the range s/λ from 2 to 100. The intrinsic length λ is introduced in eq. (15) below.

2.1.2 Results

The computed results are shown in Figs. 2 and 3. The local stress $\tau_s(x)$ decreases with growing distance from the interface down to the local yield stress $\hat{\tau}_s \approx 0$. The decrease

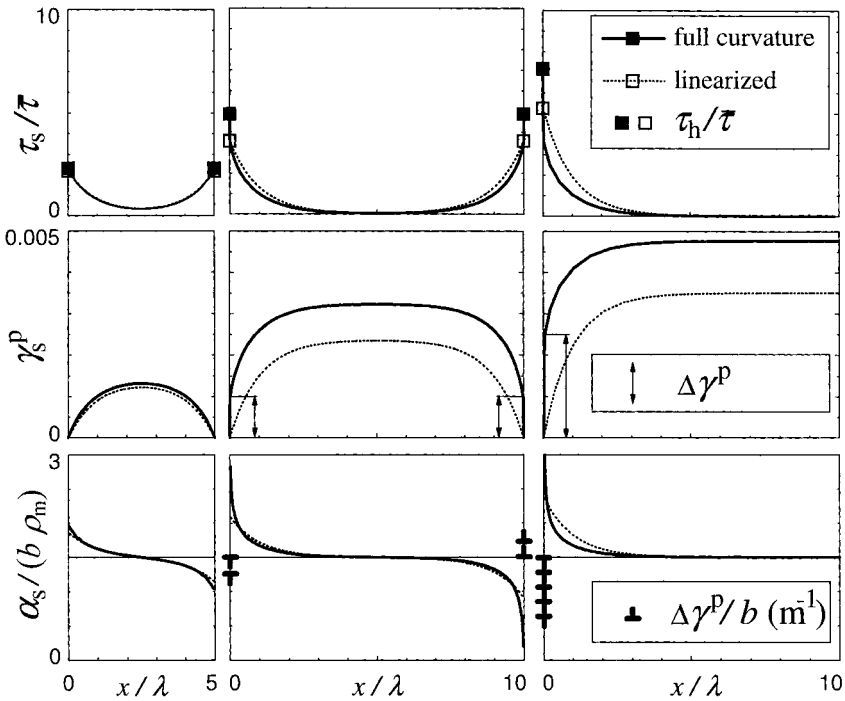

Fig. 2. Results of the numerical solution of the full curvature model (solid lines, Sec. 2.1) compared with the analytical solution of the linearized model (dotted lines, Sec. 2.2). Top: Profile of the stress in the soft phase $\tau_s(x)$ normalized by the applied stress $\bar{\tau}$ with the magnitude of the stress in the hard phase $\tau_h/\bar{\tau}$ indicated (squares). Middle: Plastic shear strain $\gamma_s^p(x)$. Bottom: Density of geometrically necessary dislocations $\alpha_s(x)$ normalized by density of mobile dislocations ϱ_m times Burgers vector b with the surface dislocation density corresponding to the step-like difference in plastic strain $\Delta\gamma^p$ indicated ($\perp$). Spacings between the hard phase s normalized by the intrinsic length λ considered are (from left to right) 5, 10, and 20, cf. Fig. 3

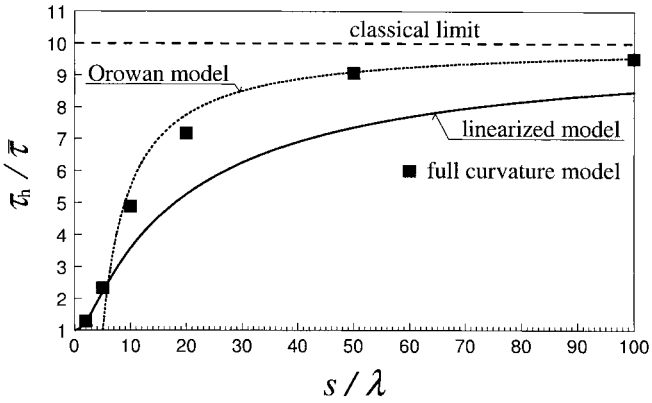

Fig. 3. Size-dependent stress in the hard phase τ_h normalized by applied stress $\bar{\tau}$ plotted against the spacing between the hard phase s normalized by the characteristic length λ. Results of the full curvature model (Sec. 2.1), linearized model (eq. $(18)_1$), Orowan model (Sec. 2.3), and classical limit (Sec. 2.4)

is enforced by the back stress in the soft phase (kinematic hardening) and compares well with experimental observations. Consider the following two examples of experimentally determined stress profiles: (i) Figure 12 in Ref. [12] showing the stress profile in subgrains formed during elevated temperature creep which corresponds to $s/\lambda \approx 60$ (subgrain size $s \approx 30$ μm, dislocation density $\varrho_m \approx 4 \times 10^{12}\,\mathrm{m}^{-2}$, intrinsic length $\lambda \approx \sqrt{1/\varrho_m} \approx 0.5\,\mu\mathrm{m}$). One should note that the values $\tau_h/\bar{\tau} \approx 10$ to 25 in Ref. [12] cannot be directly compared with the values in Fig. 3 because the volume fraction of the subgrain boundaries is much smaller than 0.1, thus pushing the stress in the boundaries upwards, eq. (7); (ii) Figure 3 in Ref. [14] showing the stress profile in a channel in PSB which corresponds to $s/\lambda \approx 4.5$ (wall-to-wall spacing $s \approx 1.4$ μm, dislocation density $\varrho_m \approx 10^{13}\ \mathrm{m}^{-2}$, intrinsic length $\lambda \approx \sqrt{1/\varrho_m} \approx 0.3\,\mu\mathrm{m}$). In this case, the experimentally found value $\tau_h/\bar{\tau} \approx 3$ agrees reasonably well with the computed value $\tau_h/\bar{\tau} \approx 2.5$, since the same volume fraction 0.1 of the hard phase was considered.

The profile of plastic shear deformation $\gamma_s^p(x)$ is directly connected to the dislocation shape, eq. (11). It shows clearly the transition from anelasticity (initial bowing of the screw dislocations) to full plastic flow (glide of the bowed-out dislocations depositing edge segments at the boundaries) with growing s/λ.

The geometrically necessary dislocations $\alpha_s(x)$, eq. (3), are represented by the edge content of the bowed-out (originally screw) mobile dislocations in the soft phase. The Burgers vector density thus formally corresponds to edge dislocations that pile-up against the interface. The layer of volume density of geometrically necessary dislocations which is responsible for the size effect concentrates in the vicinity of the interface with increasing s/λ. Moreover, a surface density of geometrically necessary dislocations appears at the interface as s/λ grows. It accommodates the step-like plastic mismatch $\Delta\gamma^p$ between the two phases, cf. [14]. The surface density of geometrically necessary dislocations thus coincides with the edge dislocations deposited at the interface in the course of the full plastic flow and increases with the growing s/λ. The geometrically necessary dislocations contribute to hardening in an organized way, namely by building-up a long-range internal back stress in the soft phase (kinematic hardening), rather

than by acting as direct obstacles to dislocation glide (isotropic hardening) as the statistically stored dislocations do, cf. [27]. This statement may need correction in multislip conditions, cf. [28].

2.2 Linearized model

To be able to discuss the proposed model in terms of simple analytical expressions, the dislocation curvature $1/R(x)$ in eq. (10) is linearized,

$$\tau_s(x)\, b + T\, \partial_x^2\, \varphi(x) = 0\,. \tag{13}$$

Strictly speaking, the linearization restricts the applicability of the model to small amplitudes of bowing ($\partial_x \varphi \ll 1$). At larger amplitudes, the linearized eq. (13) describes the shape of the dislocations qualitatively incorrectly. This is caused by the fact that the non-linear eq. (10) describes the balance of forces acting on the dislocation correctly, i.e. perpendicular to the dislocation line, whereas the linearized eq. (13) accounts only for the force component perpendicular to the x direction.

Equations (11), (12) and (13) combine, yielding a linear differential equation for the plastic deformation in the soft phase $\gamma_s^p(x)$,

$$\partial_x^2\, \gamma_s^p - \frac{1}{\lambda^2}\gamma_s^p = -\frac{\tau_h}{\lambda^2 G}\,, \tag{14}$$

with the coefficient λ (dimension of length) given by

$$\lambda = \sqrt{\frac{T}{G\varrho_m b^2}}\,. \tag{15}$$

We conclude that the enrichment of the continuum mechanics framework by considering the bowing of dislocations between the hard phase described by eq. (13) introduces the intrinsic length λ, eq. (15), into the classical model. It should be noted that eq. (13) has been originally used to introduce a length scale into a model of dislocation pattern formation [29].

The magnitude of λ can roughly be estimated by utilizing the approximate relations $T \approx Gb^2$ [25] and $1/\sqrt{\varrho_m} \approx Gb/\bar{\sigma}$, the latter corresponding to the mean distance between glide dislocations [26]. With the order-of-magnitude estimates $G \approx 10$ GPa, $b \approx 0.1$ nm and $\bar{\sigma} \approx 10$ MPa, the intrinsic length $\lambda \approx 0.1\ \mu$m results.

It is interesting to compare the intrinsic length λ, eq. (15), with the one introduced in a physically based Cosserat model of shear band formation [30]. In that model, tips of microbands of a shear band are analogous to dislocations and their spacing corresponds to the dislocation spacing. The spacing between microbands enters the expression for the Cosserat length and serves (along with an elementary amount of slip analogous to the Burgers vector) as a convenient intrinsic length scale.

2.2.1 Analytical solution

Solution to eq. (14) with boundary condition

$$\gamma_s^p\left(\pm\frac{s}{2}\right) = 0\,, \tag{16}$$

which reflects the continuity of the plastic deformation carried by the bowed dislocations reads [17, 18]

$$\gamma_{\mathrm{h}}^{\mathrm{p}} = 0\,, \qquad \gamma_{\mathrm{s}}^{\mathrm{p}}(x) = \frac{\tau_{\mathrm{h}}}{G}\left(1 - \frac{\cosh\frac{x}{\lambda}}{\cosh\frac{s}{2\lambda}}\right). \tag{17}$$

The magnitude of the solution is controlled by the stress in the hard phase τ_{h} which results from the approximate stress equilibrium (7), where the stress profile in the soft phase is given by eq. (12),

$$\tau_{\mathrm{h}} = \frac{\bar{\tau}(s+h)\cosh\frac{s}{2\lambda}}{2\lambda\sinh\frac{s}{2\lambda} + h\cosh\frac{s}{2\lambda}}\,, \qquad \tau_{\mathrm{s}}(x) = \frac{\tau_{\mathrm{h}}\cosh\frac{x}{\lambda}}{\cosh\frac{s}{2\lambda}}\,. \tag{18}$$

The lattice rotation ϕ follows from eq. (5),

$$\phi_{\mathrm{h}} = -\frac{\tau_{\mathrm{h}}}{2G}\,, \qquad \phi_{\mathrm{s}}(x) = -\frac{\tau_{\mathrm{h}}\cosh\frac{x}{\lambda}}{2G\cosh\frac{s}{2\lambda}}\,, \tag{19}$$

the lattice curvature κ from eq. (6),

$$\kappa_{\mathrm{h}} = 0\,, \qquad \kappa_{\mathrm{s}}(x) = -\frac{\tau_{\mathrm{h}}\sinh\frac{x}{\lambda}}{2G\lambda\cosh\frac{s}{2\lambda}}\,, \tag{20}$$

and the density of geometrically necessary dislocations α from eq. (3),

$$\alpha_{\mathrm{h}} = 0\,, \qquad \alpha_{\mathrm{s}}(x) = -\frac{\tau_{\mathrm{h}}\sinh\frac{x}{\lambda}}{G\lambda\cosh\frac{s}{2\lambda}}\,. \tag{21}$$

2.2.2 Results

The results are plotted and compared with the full curvature model in Figs. 2 and 3. In the range $s/\lambda \leq 5$ the solution of the linearized model almost coincides with the solution of the full curvature model. Surprisingly, the stress profile in the soft phase $\tau_{\mathrm{s}}(x)$ is relatively well described by the linearized model even for $s/\lambda > 5$. Also the distribution of the geometrically necessary dislocations in the soft phase $\alpha_{\mathrm{s}}(x)$ is relatively well accounted for by the linearized model. However, the above mentioned transition from anelasticity to full plastic flow cannot be described by the linearized model, for the dislocations cannot reach the edge orientation at the interface. Therefore, the size effect is overestimated, which is reflected by the too slow advancing of the linearized dislocation model towards the classical limit in Fig. 3.

2.3 Orowan model

If the soft phase yields fully plastically, its flow stress can be estimated as the Orowan stress, $\hat{\tau}_{\mathrm{Or}} \approx 1.5\,Gb/s$ [13], while the local yield stress of the unbounded soft phase $\hat{\tau}_{\mathrm{s}} \approx 0$ is still assumed. Given an applied stress $\bar{\tau}$, the stress in the hard phase τ_{h} results upon using the Orowan stress with the rule of mixtures [14], $\bar{\tau}(s+h) = \hat{\tau}_{\mathrm{Or}}s + \tau_{\mathrm{h}}h$. The size effect in this phenomenological description is due to the same physical mechanism (bowing of dislocations between the hard phase) as in the above non-local dislocation model, but the explicit dependence of the flow stress on the soft phase dimension is assumed a priori. This model cannot give any informa-

tion concerning the shape of the glide dislocations, stress profiles, and distribution of geometrically necessary dislocations. However, it yields an estimate of the size-dependent stress in the hard phase.

The results of the Orowan-type and dislocation-based models are compared in Fig. 3. Both the dislocation-based and the Orowan model approach the classical limit with increasing s (the volume fraction of the hard phase $h/(s+h) = 0.1$ is kept constant). The Orowan model enables a good estimate of the internal stresses in the range of widely spaced hard phase, $s/\lambda > 50$. With decreasing s/λ, τ_h should approach $\bar{\tau}$, because the dislocations cannot penetrate between the narrowly spaced hard phase. This is correctly described by the dislocation model. However, the Orowan model assumes full plastic flow of the soft phase and it is thus unable to model the mild bowing of dislocations (anelasticity): $\tau_h \to -\infty$ with decreasing s/λ.

2.4 Classical limit

The classical limit is approached on increasing the spacing s between the hard phase normalized by the intrinsic length λ, Fig. 3. In the limit cases which are (i) due to neglecting the self-energy of the bowing dislocations, $T \to 0$ (i.e. $\lambda \to 0$, eq. (15)), or (ii) due to increasing the spacing between the hard phase, $s \to \infty$, the classical composite model [14] is recovered.

This can be understood in the following way. With $T = 0$, the loops in the soft phase would not resist to curvature, so they would become square-like with their edge parts deposited directly at the interface. In other words, the volume density of geometrically necessary dislocations $\alpha_s(x)$ responsible for the size effect would condense to the surface density at the interface. Similarly, as the geometrically necessary dislocations concentrate in the vicinity of the interface with increasing s/λ, Fig. 2, they will finally condense to the classical surface density [14] in the limit $s \to \infty$.

The length of these edge dislocations deposited at the interface is given by eqs. (11), (14) with $\lambda = 0$ as $\varphi = \tau_h/(G\varrho_m b)$. Their total length per unit area of the interface, $\varphi\varrho_m$ (m^{-1}), corresponds to the surface density of the interface dislocations in the classical composite model [14]. In view of the simplifying assumption $\hat{\tau}_s \approx 0$, the plastic deformation in the soft phase then correctly results from eq. (11), $\gamma_s^p = \gamma_h^e = \tau_h/G$. Finally, the stress in the hard phase follows from eq. (7), $\tau_h = \bar{\tau}(s+h)/h$. Comparing this classical result with eq. $(18)_1$, we see that the size effect has disappeared and only the volume-fraction dependence remains, cf. Fig. 3.

3. Cosserat Model

Still in the Voigt approximation, a linear one-dimensional Cosserat medium will be considered and applied to the two-phase structure sheared in parallel. It will appear that an identification with the above linearized dislocation model is possible, since the governing equations derived below have the same mathematical structure.

3.1 Cosserat continuum

A one-dimensional Cosserat continuum described by the material displacement field $u_x = \bar{\gamma} y$ and a rotation field $\Phi = \Phi_z(x)$ is considered. The non-zero components of the

Cosserat deformation tensor (B1) are

$$\begin{aligned} e_{xy} &= \bar{\gamma} + \Phi\,, \\ e_{yx} &= -\Phi\,. \end{aligned} \tag{22}$$

The curvature of the medium $k = k_{zx}$ is, cf. eq. (B2),

$$k = \partial_x \Phi\,. \tag{23}$$

The relation (B3) for the couple stress $\mu = \mu_{zx}$ becomes

$$\partial_x \mu - (\sigma_{xy} - \sigma_{yx}) = 0\,. \tag{24}$$

At first, we are not able to distinguish between the elastic and plastic parts of the material deformation. The Cosserat framework is therefore tentatively completed by linearized material constitutive equations,

$$\begin{aligned} \sigma_{xy} &= 2\bar{G}\frac{\bar{\gamma}}{2} + 2\bar{G}_{\mathrm{C}}\left(\frac{\bar{\gamma}}{2} + \Phi\right), \\ \sigma_{yx} &= 2\bar{G}\frac{\bar{\gamma}}{2} - 2\bar{G}_{\mathrm{C}}\left(\frac{\bar{\gamma}}{2} + \Phi\right), \end{aligned} \tag{25}$$

$\bar{G}$ is a classical material (secant) shear modulus, $\bar{G}_{\mathrm{C}}$ its Cosserat counterpart. In eqs. (25), one recognizes the symmetric and skew-symmetric parts of the Cosserat deformation tensor (22). The couple stress μ is also related to the curvature k of the Cosserat medium (23) by a linearized constitutive equation,

$$\mu = 4\bar{G}_{\mathrm{C}}\, l^2\, k\,, \tag{26}$$

l is a Cosserat intrinsic length.

3.2 Identification with the dislocation model

The Cosserat framework will now be applied to the one-dimensional two-phase periodic structure sheared in parallel. As it is a priori clear that the non-classical behaviour must be related to plasticity which is in the present model restricted to the soft phase, the hard phase remains classically elastic, cf. eq. (9),

$$\bar{\gamma} = \frac{\tau_{\mathrm{h}}}{G}\,. \tag{27}$$

Equations (23) to (27) now yield a differential equation for the Cosserat rotation Φ,

$$\partial_x^2 \Phi - \frac{1}{l^2}\,\Phi = \frac{\tau_{\mathrm{h}}}{2l^2 G}\,. \tag{28}$$

This equation has the same form as eq. (14) which describes the profile $\gamma_{\mathrm{s}}^{\mathrm{p}}(x)$ of the plastic shear in the soft phase in the non-local dislocation model. Comparing the two equations, we see that the Cosserat intrinsic length l equals the intrinsic length λ of the dislocation model,

$$l = \lambda\,, \tag{29}$$

and that the Cosserat rotation Φ is the axial vector of plastic rotation in the soft phase,

$$\Phi(x) = -\frac{1}{2}\,\gamma_{\mathrm{s}}^{\mathrm{p}}(x)\,, \tag{30}$$

cf. eq. (5). Thus, the Cosserat rotation Φ appears to be fully plastic. In view of the decomposition (2), we are now able to separate the elastic and plastic parts of the Cosserat deformation tensor **e**, eq. (22),

$$\begin{aligned} e^{\mathrm{e}}_{xy} &= \gamma^{\mathrm{e}}\,, \qquad e^{\mathrm{p}}_{xy} = \gamma^{\mathrm{p}} + \Phi\,, \\ e^{\mathrm{e}}_{yx} &= 0\,, \qquad e^{\mathrm{p}}_{yx} = -\Phi\,. \end{aligned} \tag{31}$$

As for the curvature of the Cosserat medium k, it is fully plastic as well, and it follows from eqs. (23), (30) and in view of eqs. (2), (6) that it is the negative of the lattice curvature κ,

$$k = -\kappa\,. \tag{32}$$

3.3 Elastic Cosserat model

It turns out that in the present application, it is sufficient to consider elastic constitutive relations alone to get an even more straightforward identification with the dislocation model. To understand this, consider the material constitutive eqs. (25) and recognize that (i) $\bar{\gamma}/2 + \Phi = -\phi$, cf. eqs. (2), (5), (30) and (ii) the term $\bar{G}\bar{\gamma}$ played no role in deriving eq. (28). The elastic constitutive equations are

$$\begin{aligned} \sigma_{xy} &= 2G\frac{\gamma^{\mathrm{e}}}{2} - 2G_{\mathrm{C}}\phi\,, \\ \sigma_{yx} &= 2G\frac{\gamma^{\mathrm{e}}}{2} + 2G_{\mathrm{C}}\phi\,, \end{aligned} \tag{33}$$

where the skew-symmetric part of the elastic Cosserat deformation tensor (31) was re-written with the help of eq. (5). G is the classical elastic shear modulus, G_{C} is its Cosserat counterpart. In view of eqs. (26), (29), (32), the couple stress μ can be related to the lattice curvature κ using the intrinsic length λ,

$$\mu = -4G_{\mathrm{C}}\lambda^2\kappa\,. \tag{34}$$

The material relation (23) is replaced by the elastic relation (6). From eqs. (24), (33), (34) and (6), a differential equation for the lattice rotation in the soft phase follows,

$$\partial_x^2\phi - \frac{1}{\lambda^2}\phi = 0\,. \tag{35}$$

From eqs. (5) and (27), eq. $(19)_1$ can be deduced. Accordingly, the boundary condition

$$\phi\left(\pm\frac{s}{2}\right) = -\frac{\tau_{\mathrm{h}}}{2G} \tag{36}$$

reflects continuity of the lattice rotation across the soft/hard phase interface. Solution to eq. (35) with boundary condition (36) reproduces the result $(19)_2$. The elastic shear in the soft phase now follows from eq. (5) and the plastic one from the decomposition (2). The shear stress in the hard phase τ_{h} follows from the approximate stress equilibrium (B4) which takes the form

$$\frac{1}{2(s+h)}\int_{\langle s+h\rangle}(\sigma_{xy}(x) + \sigma_{yx}(x))\,\mathrm{d}x = \bar{\tau}\,, \tag{37}$$

with σ_{xy} and σ_{yx} being given by eqs. (33). It can be checked easily that the result $(18)_1$ is reproduced. Similarly, the lattice curvature κ, eq. (20), and the density of geometri-

cally necessary dislocations α, eq. (21), follow correctly from the elastic Cosserat model. The Cosserat elastic modulus G_C and therefore the couple stress μ, however, remain undetermined by the above interpretation of the Cosserat framework. To be able to identify G_C, more complex dislocation distributions must be imagined, cf. [31].

4. Concluding Remarks

A simple continuum mechanics model of plastic deformation of two-phase materials has been recalled in Section 2. It has been shown that the self-energy (line tension) of dislocations bowing between the plastically hard phase renders the model non-local. With increasing spacing s between the hard phase, the non-local behaviour starts with the initial mild bowing of dislocations (anelasticity), covers the range of full plastic flow (large bowing of dislocations depositing segments at the interfaces), and approaches the size-independent classical limit, Figs. 2 and 3. Because of the non-linear expression for the dislocation curvature in eq. (10), the equations of the full model have been solved numerically. In order to discuss the results in terms of analytical expressions, the analytical solution of the linearized model with eq. (13) replacing eq. (10) has been given as well. Strictly speaking, the linearized model correctly describes only mild bowing of dislocations between the hard phase (anelasticity). Although the linearized model overestimates the size effect for large bowing of dislocations (plasticity), cf. Fig. 3, the comparison in Fig. 2 showing that it accounts reasonably well for the size-dependent distributions of stresses, strains, lattice rotations, and geometrically necessary dislocations, justifies the discussion.

The non-local effect is introduced into the linearized model via the second-order plastic strain gradient in eq. (14). With the usual estimate of line tension $T \approx Gb^2$ [25], the intrinsic length λ, eq. (15), equals the mean spacing between mobile dislocations $\lambda \approx 1/\sqrt{\varrho_m}$. Thus, contrary to the conventional strain gradient theories, the intrinsic length varies in the course of plastic deformation. Since the width of the soft phase s corresponds to the characteristic length of the deformation field, the size-dependent response is determined by the ratio s/λ.

An interpretation of the Cosserat intrinsic length scale, rotation and curvature has been proposed, based on comparison of the linearized dislocation-based model with the Cosserat model introduced in Section 3. The intrinsic length λ resulting from the dislocation-based model directly determines the Cosserat intrinsic length l, eq. (29). The Cosserat rotation Φ has been identified as the axial vector of plastic rotation caused by the bowing of dislocations in the soft phase, eq. (30). Because of the strong coupling between elastic and plastic shear, eq. (2), the Cosserat model could also be formulated entirely in the Cosserat-elastic framework. Then, the Cosserat rotation equals the elastic lattice rotation ϕ, the Cosserat curvature is the lattice curvature κ. The Cosserat elastic modulus G_C could not be identified and therefore the couple stress μ remains undetermined, suggesting that the Cosserat model is still more general than the proposed dislocation-based model which is actually reminiscent of the gradient theory with symmetric stress tensor [7].

Acknowledgements R. S. gratefully acknowledges inspiring discussions with Profs. Blum, Kratochvíl and Mughrabi, their comments on the manuscript, and access to Refs. [27, 28, 30] prior to publication, as well as the financial support by the Deutsche Forschungsgemeinschaft.

Appendix A Continuum Theory of Dislocations

In the classical continuum theory of dislocations [20], the compatible material deformation is described by a continuous and differentiable displacement field $\mathbf{u}$. The displacement gradient $\boldsymbol{\beta}$,

$$\boldsymbol{\beta} = \operatorname{grad} \mathbf{u}\,, \qquad \beta_{ij} = \partial_j u_i\,, \tag{A1}$$

consists of an elastic and a plastic part,

$$\boldsymbol{\beta} = \boldsymbol{\beta}^{\mathrm{e}} + \boldsymbol{\beta}^{\mathrm{p}}\,, \qquad \beta_{ij} = \beta^{\mathrm{e}}_{ij} + \beta^{\mathrm{p}}_{ij}\,. \tag{A2}$$

The former yields the dislocation density tensor $\boldsymbol{\alpha}$ in the form

$$\boldsymbol{\alpha} = \operatorname{curl} \boldsymbol{\beta}^{\mathrm{e}}\,, \qquad \alpha_{jm} = \epsilon_{klm}\partial_l \beta^{\mathrm{e}}_{jk}\,, \tag{A3}$$

where ϵ_{klm} is the Levi-Civita permutation tensor. The elastic part of the displacement gradient (and, similarly, the plastic one) can be decomposed into the symmetric elastic material strain ε^{e} and the skew-symmetric elastic material rotation $\boldsymbol{\omega}^{\mathrm{e}}$,

$$\boldsymbol{\beta}^{\mathrm{e}} = \boldsymbol{\varepsilon}^{\mathrm{e}} + \boldsymbol{\omega}^{\mathrm{e}}\,, \qquad \beta^{\mathrm{e}}_{ij} = \varepsilon^{\mathrm{e}}_{ij} + \omega^{\mathrm{e}}_{ij}\,. \tag{A4}$$

The axial vector $\boldsymbol{\phi}$ of the elastic rotation describes the rotation of the lattice,

$$\boldsymbol{\phi} = \overset{\times}{\boldsymbol{\omega}}{}^{\mathrm{e}}\,, \qquad \phi_m = -\frac{1}{2}\epsilon_{klm}\omega^{\mathrm{e}}_{kl}\,. \tag{A5}$$

Lattice curvature $\boldsymbol{\kappa}$ follows in the form

$$\boldsymbol{\kappa} = \operatorname{grad} \boldsymbol{\phi}\,, \qquad \kappa_{ij} = \partial_j \phi_i\,. \tag{A6}$$

The stress tensor $\boldsymbol{\sigma}$ is symmetric,

$$\boldsymbol{\sigma} = \boldsymbol{\sigma}^{\mathrm{T}}\,, \qquad \sigma_{ij} = \sigma_{ji}\,. \tag{A7}$$

Stress equilibrium reads

$$\operatorname{div} \boldsymbol{\sigma} = 0\,, \qquad \partial_j \sigma_{ij} = 0\,. \tag{A8}$$

As the average of internal stresses vanishes in an infinitely extended medium, the average stress equals the applied one,

$$\lim_{V\to\infty} \frac{1}{V}\int_V \sigma_{ij}\,\mathrm{d}V = \bar{\sigma}_{ij}\,. \tag{A9}$$

Appendix B Cosserat Continuum

Cosserat continuum is described by the displacement field $\mathbf{u}$ and an independent rotation field $\boldsymbol{\Phi}$. The Cosserat deformation tensor reads

$$\mathbf{e} = \operatorname{grad} \mathbf{u} + \boldsymbol{\varepsilon}\boldsymbol{\Phi}\,, \qquad e_{ij} = \partial_j u_i + \epsilon_{ijk}\Phi_k\,. \tag{B1}$$

The curvature $\mathbf{k}$ of the medium is related to the rotation field,

$$\mathbf{k} = \operatorname{grad} \boldsymbol{\Phi}\,, \qquad k_{ij} = \partial_j \Phi_i\,. \tag{B2}$$

Rather than the symmetry of the force stress tensor (A7), the balance of moment of momentum now yields a relation for the couple stress $\boldsymbol{\mu}$,

$$\operatorname{div} \boldsymbol{\mu} + 2\overset{\times}{\boldsymbol{\sigma}} = 0\,, \qquad \partial_j \mu_{ij} - \epsilon_{ijk}\sigma_{jk} = 0\,, \tag{B3}$$

$\overset{\times}{\boldsymbol{\sigma}}$ is the axial vector of the skew-symmetric part of the force stress tensor $\boldsymbol{\sigma}$. The stress equilibrium (A8) still holds. In the two-phase model, the applied averaged stress is symmetric, $\bar{\sigma}_{ij} = \bar{\sigma}_{ji}$. It equals the average of the symmetric part of the force stress tensor in the infinitely extended medium [32],

$$\lim_{V\to\infty} \frac{1}{2V} \int_V \left(\sigma_{ij} + \sigma_{ji}\right) \mathrm{d}V = \bar{\sigma}_{ij} \,. \tag{B4}$$

References

[1] N. A. FLECK, G. M. MULLER, M. F. ASHBY, and J. W. HUTCHINSON, Acta Metall. et Mater. **42**, 475 (1994).
[2] N. A. FLECK and J. W. HUTCHINSON, Adv. Applied Mechanics **33**, 295 (1997).
[3] N. A. FLECK and J. Y. SHU, in: Modelling of Structure and Mechanics of Materials from Microscale to Product, Proc. 19th Risø Internat. Symp. Materials Science, Eds. J. V. CARSTENSEN, T. LEFFERS, T. LORENTZEN, O. B. PEDERSEN, B. F. SØRENSEN, and G. WINTHER, 1998 (pp. 91–96).
[4] S. FOREST, G. CAILLETAUD, and R. SIEVERT, Arch. Mech. **49**, 705 (1997).
[5] S. FOREST, Acta Mater. **46**, 3265 (1998).
[6] M. F. ASHBY, Phil. Mag. **21**, 399 (1970).
[7] H. M. ZBIB, in: Material Instabilities in Solids, Proc. IUTAM Symp. Material Instabilities, Eds. R. DE BORST and E. VAN DER GIESSEN, John Wiley and Sons, New York 1998 (pp. 473–487).
[8] M. RHEE, J. P. HIRTH, and H. M. ZBIB, Acta Metall. et Mater. **42**, 2645 (1994).
[9] K. SHIZAWA and H. M. ZBIB, Internat. J. Plasticity **15**, 899 (1999).
[10] E. GÖTTLER, Phil. Mag. **28**, 1057 (1973).
[11] M. A. MORRIS and J. L. MARTIN, Acta Metall. **32**, 549 (1984).
[12] M. A. MORRIS and J. L. MARTIN, Acta Metall. **32**, 1609 (1984).
[13] H. MUGHRABI, in: Continuum Models of Discrete Systems, Eds. O. BRULIN and R. K. T. HSIEH, North-Holland Publ. Co., Amsterdam 1981 (pp. 241–257).
[14] H. MUGHRABI, Acta Metall. **31**, 1367 (1983).
[15] H. MUGHRABI, phys. stat. sol. (a) **104**, 107 (1987).
[16] O. B. PEDERSEN, Acta Metall. **35**, 2567 (1987).
[17] R. SEDLÁČEK, phys. stat. sol. (a) **149**, 85 (1995).
[18] R. SEDLÁČEK, Mater. Sci. Eng. A **234-236**, 643 (1997).
[19] R. SEDLÁČEK, phys. stat. sol. (b) **201**, R5 (1997).
[20] E. KRÖNER, Kontinuumstheorie der Versetzungen und Eigenspannungen, Springer-Verlag, Berlin 1958.
[21] J. F. NYE, Acta Metall. **1**, 153 (1953).
[22] D. PEIRCE, R. J. ASARO, and A. NEEDLEMAN, Acta Metall. **30**, 1087 (1982).
[23] R. SEDLÁČEK, Phil. Mag. Lett. **76**, 275 (1997).
[24] H. PRESS, B. P. FLANNERY, S. A. TEUKOLSKY, and W. T. VETTERLING, Numerical Recipes, Cambridge University Press, Cambridge 1989.
[25] J. P. HIRTH and J. LOTHE, Theory of Dislocations, John Wiley and Sons, 1982.
[26] W. BLUM, in: Plastic Deformation and Fracture of Materials, Ed. H. MUGHRABI, Vol. 6 of Materials Science and Technology, Eds. R. W. CAHN, P. HAASEN, and E. J. KRAMER, VCH Verlagsgesellschaft, Weinheim 1993 (pp. 359–405).
[27] H. MUGHRABI, in: Deformation-Induced Microstructures: Analysis and Relation to Properties, Proc. 20th Risø Internat. Symp. Materials Science, Eds. J. B. BILDE-SØRENSEN, J. V. CARSTENSEN, N. HANSEN, D. JUUL JENSEN, T. LEFFERS, W. PANTLEON, O. B. PEDERSEN, and G. WINTHER, 1999 (pp. 417–426).
[28] H. MUGHRABI, Mater. Sci. Eng. A, in press.
[29] J. KRATOCHVÍL and M. SAXLOVÁ, Scripta Metall. et Mater. **26**, 113 (1992).
[30] J. KRATOCHVÍL, E. LABBÉ, C. REY, and S. YANG, Scripta Mater. **41**, 761 (1999).
[31] R. B. PECHERSKY, in: CISM Course on Postcritical Behaviour and Fracture of Dissipative Solids, Ed. R. B. PECHERSKY, Udine 1988.
[32] S. FOREST, R. DENDIEVEL, and G. CANOVA, Modelling Simul. Mater. Sci. Eng. **7**, 829 (1999).